Parametric Amplification in a Superconducting Microstrip Transmission Line

Wenlei Shan, *Member, IEEE*, Yutaro Sekimoto, and Takashi Noguchi

***Abstract*—Broadband parametric amplifiers (PAs), which utilize the nonlinear kinetic inductance of superconducting transmission lines, provide new access to ultimate sensing capability for radio astronomical observation and microwave quantum electronics. In this paper, the parametric amplification is investigated with a time-domain numerical method. The results present direct images of the traveling waves, which clarify the distinctively different features of the parametric gain in uniform and impedance-perturbed nonlinear transmission lines. The results indicate that the traveling-wave PAs (TWPAs) are susceptible to impedance mismatching because of the lack of isolation between the input and the output ports. In the experimental part of this paper, we tested, for the first time, microstrip TWPAs based on NbTiN. A parametric gain was observed at liquid helium temperature.**

***Index Terms*—Finite-difference methods, microstrip, parametric amplifiers (PAs), shock waves, superconducting transmission lines.**

I. Introduction

PARAMETRIC amplifiers (PAs) perform frequency mixing between a weak signal and a strong pump using reactors (capacitors or inductors, lumped or distributed) with their parametric reactance being modulated by the pump. If the mixers are properly designed and operated, the power of the pump can be transferred to the signal frequency, thus resulting in the amplification of the signal. Since pure reactors are intrinsically lossless, PAs are less affected by electric noise than semiconductor transistor amplifiers. PAs have various forms, among which the most sensitive PAs are made of superconductors. PAs utilizing Josephson junctions operating at centimeter wavelengths, which were intensively investigated in the 1970s, demonstrated noise temperatures of 20–50 K [1]–[3]. In present days, the development of superconducting quantum manipulation and radio astronomical observation leads to renewed interests in PAs. State-of-the-art Josephson junction PAs have approached the quantum limit at microwave frequency [4]–[6].

Manuscript received January 4, 2016; revised March 30, 2016; accepted April 6, 2016. Date of publication April 21, 2016; date of current version June 17, 2016. This work was supported in part by the National Natural Science Foundation of China under Grant U1331203. This paper was recommended by Associate Editor A. Kleinsasser.

W. Shan is with the Purple Mountain Observatory, Chinese Academy of Sciences, Nanjing 210008, China, and also with the National Astronomical Observatory of Japan, Tokyo 181-8588, Japan (e-mail: shan@pmo.ac.cn).

Y. Sekimoto and T. Noguchi are with the National Astronomical Observatory of Japan, Tokyo 181-8588, Japan (e-mail: sekimoto.yutaro@nao.ac.jp; Takashi.Noguchi@nao.ac.jp).

Color versions of one or more of the figures in this paper are available online at http://ieeexplore.ieee.org.

Digital Object Identifier 10.1109/TASC.2016.2555914

In the early years, several disadvantages caused limitations for the practical uses of conventional PAs, among which the narrow bandwidth is the most distinct one. Extracting the energy from a lumped nonlinear reactor is not effective unless the reactor is tuned out. The tuning circuit behaves as a bandpass filter and results in typically a 0.1% fractional bandwidth, not sufficient for broadband applications. Another drawback appears if a PA is a reflection-type, in which a circulator is utilized to separate the input signal from the output signal. The circulator contributes noise, and its bulk size causes difficulties in building a compact system as well. Thus, instead of circulators, transmission-type resonators were employed [4], [7], although their bandwidths are still narrow.

To broaden the bandwidth, phase-insensitive superconducting traveling-wave PAs (TWPAs) are newly developed [8]–[10]. The optical analog of a TWPA is an optical parametric amplifier (OPA). Both of them are based on the mechanism of four-photon mixing. A TWPA is basically a nonlinear transmission line through which the signal progressively gains power from the pump during propagating. The first superconducting TWPA in the form of a coplanar line waveguide was demonstrated at 0.3 K with a gain of about 15 dB [8]. Cascading two of the amplifiers exhibits a gain as high as 30 dB and a 3-dB fractional bandwidth of 40% [9]. Recently, TWPAs implemented using Josephson junctions as parametric inductors approached quantum-limited noise along with a broad bandwidth [10].

The frequency-domain analysis of the superconducting TWPA is established based on the four-photon mixing theory [8], which is almost identical to that developed for OPAs [11]. With the assumption that the transmission line is homogeneous and impedance matched in both ends, the four-photon mixing theory predicts an exponential parametric gain under the condition that the phase shift induced by the nonlinearity (related to the pump power) can be completely compensated by the linear dispersion of the transmission line (irrelevant to the pump power). The phase-matching requirement for an OPA can be satisfied with the use of the high-order dispersion of highly nonlinear fibers. However, for superconducting TWPAs, in which the dielectric layer is dispersionless, the linear dispersion is produced by using photonic band-gap structures [8], [10], [12], also called dispersion engineering. In addition to producing anomalous dispersion, photonic band-gap structures are adopted for preventing the occurrence of shock waves by suppressing the third harmonic generation [8]. In fact, both of the aforementioned techniques violate the homogeneity of the transmission line, and thus, the analytical method is not strictly applicable. Accurate and robust analysis can be performed

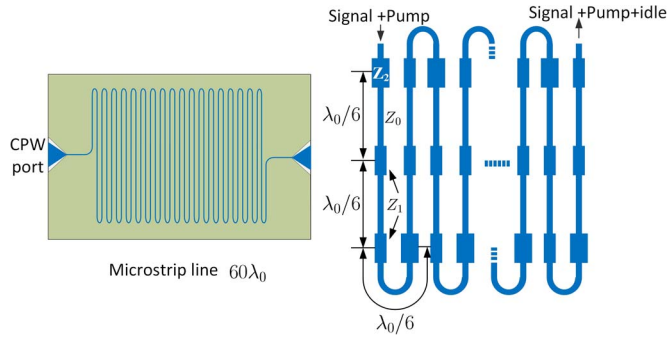

Fig. 1. Schematic of the microstrip superconducting TWPA under study. The overview diagram is shown on the left side, and the detailed arrangement of the impedance perturbations is illustrated on the right side.

by numerically solving the nonlinear telegraph equations. For instance, a finite-difference time-domain (FDTD) method has been used to calculate the broadband gain profile of superconducting TWPAs [13]. In our research, we also developed an FDTD method, but particularly focused on the evolution of the waveforms both of the pump and the signal in the nonlinear transmission line, from which we can inspect the superconducting TWPAs in a straightforward point of view.

The already reported superconducting TWPAs are implemented with a coplanar waveguide (CPW) [8], [9]. These devices have apparent advantages in that transmission loss is low and fabrication is simple, but their characteristic impedances are two or three times higher than 50 Ω, consequently causing difficulties in broadband impedance matching. By contrast, it is not difficult to fabricate 50-Ω superconducting microstrip lines. Furthermore, because of the large kinetic inductance ratio, the wave velocity in microstrip lines is much lower than in a CPW, and therefore, the physical length needed for the same amplitude of gain is much shorter. Technically motivated by these reasons, we choose NbTiN microstrip lines as the nonlinear media of the amplifier in the experimental part of this paper.

II. Numerical Analysis

A. Simulation Method

Before writing down the nonlinear telegraph equations for the superconducting TWPA to be investigated in this paper, we illustrate its architecture in Fig. 1. The backbone structure is a homogeneous transmission line with characteristic impedance of Z_0. This transmission line can be regarded as a distributed frequency mixer pumped by a strong sinusoidal wave at frequency f_0 (corresponding to the wavelength of λ_0), along with a weak signal at f_s. There are two sets of impedance perturbations applied to the homogeneous line. Evenly spaced by $\lambda_0/6$, impedance perturbations of Z_1 are loaded to suppress the third harmonic generation. On the basis of the previous loadings, every $\lambda/2$ in distance, the impedance perturbation is replaced by Z_2 in order to introduce anomalous dispersion [8]. The length of each node is chosen to be $\lambda_0/30$ in our simulation and experiment. A minor change in this length does not bring a significant difference to the results.

The numerical model for this nonlinear and inhomogeneous transmission line is the well-known telegraph equations, taking nonlinearity and nonuniformity into consideration, i.e.,

$$\frac{\partial V}{\partial t} = -\frac{1}{C(z)}\frac{\partial I}{\partial z} \tag{1}$$

$$\frac{\partial I}{\partial t} = -\frac{1}{L(z)}(1+\rho I^2)^{-1}\frac{\partial V}{\partial z}. \tag{2}$$

The current and voltage at position z are normalized by the pumping current I_p and $Z_0 I_p$, respectively. The time is normalized by f_0^{-1}, and the length is normalized by λ_0. The capacitance $C(z)$ and inductance $L(z)$ per unit length are normalized by the values for the unperturbed part of the transmission line with a characteristic impedance of Z_0. The characteristic impedance of the line at z is $Z(z) = \sqrt{L(z)/C(z)}$. The nonlinearity coefficient is defined as

$$\rho = 3\eta\frac{I_p^2}{I_c^2} \tag{3}$$

where I_c is the critical current of the conducting strip of the unperturbed part of the microstrip line, and η is the kinetic inductance ratio. For a microstrip line with the dielectric layer much thinner than the penetration depth of the superconducting layers, it is close to 1. Compared with the notations in [8] and [11], where the nonlinear phase shift per wavelength γ is used, we find that the correspondence is $\gamma = \pi\rho/4$. If the transmission line is not homogeneous or is mismatched at both ends, there will be backward traveling waves. The forward and backward propagating waves for the current can be separated by

$$a = V/Z + I \tag{4}$$

$$b = V/Z - I \tag{5}$$

where a and b are the forward and backward current waves, respectively. The voltage wave can be treated in a similar way.

The following numerical method is used for tracking the evolution of waves in the nonlinear transmission line by solving (1) and (2). We adopt an FDTD algorithm using the staggered leapfrog scheme [14], which is second-order accurate in both space and time. In this scheme, the current and voltage are differentiated in two sets of lattices, which are staggered in space and time by half-step. The finite-difference approximations of (1) and (2) are

$$\frac{V_j^{n+1/2} - V_j^{n-1/2}}{\Delta t} = -\frac{1}{C_j}\frac{I_{j+1/2}^n - I_{j-1/2}^n}{\Delta x} \tag{6}$$

$$\frac{I_{j+1/2}^{n+1} - I_{j+1/2}^n}{\Delta t} = -\frac{1}{L_{j+1/2}}\frac{V_{j+1}^{n+1/2} - V_j^{n+1/2}}{\Delta x} \times \left[1+\rho\left(\frac{I_{j+1/2}^{n+1} - I_{j+1/2}^n}{2}\right)^2\right]^{-1}. \tag{7}$$

Equation (7) is a cubic equation for $I_{j+1/2}^{n+1}$ and can be used as an iteration equation to solve for $I_{j+1/2}^{n+1}$. In practice, convergence of this iteration is always rapidly achieved. This finite-difference method becomes unstable when a steep shock wave occurs. To avoid this instability, we add numerical dissipation to the voltage in (6) as

$$V_j^{n+1/2} \leftarrow V_j^{n+1/2} + \xi \left(V_{j+1}^{n-1/2} - 2V_j^{n-1/2} + V_{j-1}^{n-1/2} \right) \quad (8)$$

where $\xi \ll 1$ is a small number. Because of (8), high-order harmonics dissipate and slightly damp the shock wave. As for the boundary conditions, at the output and input ports, $V/I = Z_L$ and $V/(I_s' - I) = Z_s$, are used, respectively, where Z_L and Z_s are the normalized load and source impedance, respectively, and $I_s' = I_p \cos \omega_p t + I_s \cos \omega_s t$, i.e., the source current, which includes the driving pump and the weak signal. It is noted that in applying the boundary conditions, the two sets of lattices have to be extrapolated by $\Delta x/2$ to the edge of the line.

The forward wave a or the backward wave b is a mixture of single-frequency continuous waves at f_0, f_s, and f_i and the harmonics of the pump. Supposing that the small-signal response is linear, we can extract the signal–image combination from the mixture by subtracting from the mixture an independently simulated waveform driven by pure pump. To separate the signal and the image, we utilize the sideband separation technique, as is briefed in following. For four-photon mixing, the frequencies obey the following rule:

$$f_i = 2f_0 - f_s. \quad (9)$$

Accordingly, the phases follow:

$$\phi_i = 2\phi_0 - \phi_s + \text{Const.} \quad (10)$$

Bearing this phase relation in mind and adopting the quadrature mixing technique [16], we calculate the forward waveform $a_{\phi_0=0}$ with the initial phase of the pump equaling to zero, and the waveform $a_{\phi_0=\pi/2}$ with the phase of the pump rotated by 90°, and then we can perform the separation by

$$a_{s,\phi_0=0} = \frac{a_{\phi_0=0} + a_{\phi_0=\pi/2}}{2} \quad (11)$$

$$a_{i,\phi_0=0} = \frac{a_{\phi_0=0} - a_{\phi_0=\pi/2}}{2}. \quad (12)$$

The backward wave can be calculated in the same way.

B. Simulation Results

We simulated a nonlinear transmission line with an overall length of $60\lambda_0$, which is the nominal length of the microstrip superconducting TWPAs in our experiment. In the simulation, we assume that the nonlinear coefficient $\rho = 0.1$ is equivalent to the pumping current of 18% of I_c. We also assume that the transmission line is impedance matched at both input and output ports and leave the unmatched condition at the end of this section. The performance of the TWPA depends on how the impedance perturbation is applied. Three different conditions are investigated in detail.

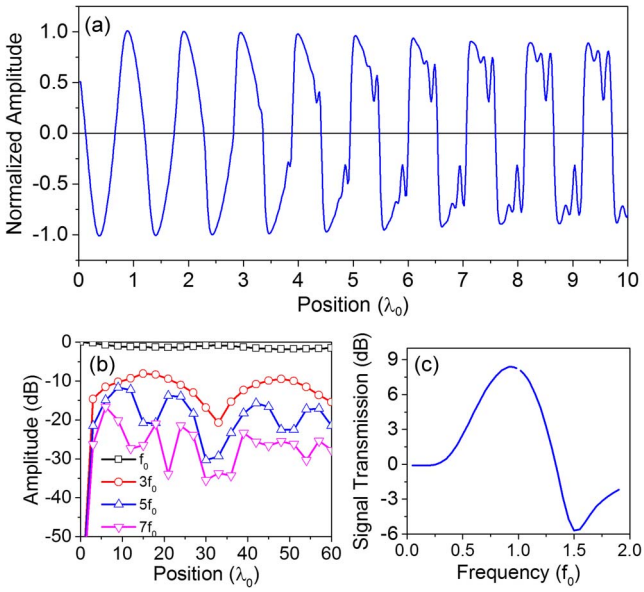

Fig. 2. Traveling-wave properties of a superconducting transmission line with an increasing parametric inductance $L = L_0(1 + \rho I^2)$. (a) Current waveform within the distance of the first $10\lambda_0$, driven by a sinusoidal oscillation at $z = 0$. (b) Amplitudes of the pump and its harmonics as a function of distance along the line. (c) Parametric gain as a function of signal frequency for a transmission distance of $60\lambda_0$ and nonlinear coefficient $\rho = 0.1$. Note that the signal cannot be distinguished from the pump when f_s is close to f_0 due to insufficient spectrum resolution in the fast Fourier transform (FFT) process. Therefore, a small gap around $f_s = 1$ appears.

1) Homogeneous Nonlinear Transmission Line: In this case, the transmission line is free from any impedance perturbation, i.e., $Z_1 = Z_2 = Z_0$. The parametric amplification in such a nonlinear transmission line has been analytically investigated [15], [17], and a pessimistic conclusion was reached, which asserted that there is no parametric gain in a nonlinear transmission line because of the arising of dissipating shock waves. However, we found that this conclusion is correct only in the case that the parametric reactance is a monotonically decreasing function of the pump amplitude. In the case of a superconducting nonlinear transmission line whose inductance is a monotonically increasing function of the pumping current, as given by $L = L_0(1 + \rho I^2)$, we indeed get a notable parametric gain even in the presence of shock waves.

Fig. 2(a) shows a snapshot of the traveling waves propagating from left to right within the distance of the first $10\lambda_0$. Each part of the traveling wave, which can be regarded as a voltage impulse with the height equaling to the local amplitude, propagates along the line at a speed of $v = v_0/\sqrt{1 + \rho I^2}$, where v_0 is the phase velocity when nonlinearity disappears [15]. Because the traveling speed is lower for an impulse with a larger amplitude, the sinusoidal waveform gradually deforms. The slope of the waveform becomes progressively steeper at the trailing side of positive and negative half-waves, and shock waves form if $d|I|/dz$ becomes infinitely large. In practice and also in this numerical simulation, however, the discontinuity of current cannot happen because of damping at high-order harmonics and inertial effects associated with the superconducting current flow [19]. For this reason, shock waves and their effects can be numerically simulated.

Because the parametric inductance is a cubic function of the current, only odd harmonics are generated. We perform FFT for the temporal waves at different positions along the line, and the relative amplitudes of the third, fifth, and seventh harmonic tones are shown in Fig. 2(b). The maximum amplitudes of the third and fifth harmonics are -8.1 and -11.7 dB, respectively. In comparison with the maximum harmonic conversion efficiency of $1/n^2$ for a nonlinear resistive element [20], where n is the harmonic number, the efficiency is 1.4 and 2.3 dB larger. This comparison reveals the potential usage of a nonlinear transmission line as a harmonic generator. It is worth noting that the pump tone and its harmonics are quasi-periodic functions of the position. It is found that the waveform tends to restore to the sinusoidal waveform about every $32\lambda_0$ in distance. This indicates that the transmission loss of the harmonics is insignificant.

The parametric gain of a small signal for this $60\lambda_0$-long transmission line is shown in Fig. 2(c). The gain profile is asymmetrical around the pump, with the highest gain of about 8 db and 3 dB bandwidths about 40%, and squeezing is found at $f = 1.5$.

It is of interest to verify that there will be no parametric gain if the inductance is a monotonically decreasing function of the current, as argued by Landauer in [15] and [17]. He pointed out that, for a decreasing parametric reactance, the shock front keeps dissipating energy. To verify his conclusion, we simulate the parametric amplification of an artificial nonlinear transmission line with the same nonlinearity coefficient, i.e., $\rho = 0.1$, but different inductance, i.e., $L = L_0(1 - \rho I^2)$. The only difference between the two cases is the sign of ρ. Fig. 3(a) shows the traveling wave within the distance of the first $10\lambda_0$. In contrast to Fig. 2(a), shock waves in Fig. 3(a) appear at the leading part of each positive and negative of half-waves, with more energy concentrating on the shock front. Much stronger harmonics are generated, as shown in Fig. 3(b), in which the fifth harmonic generation is particularly efficient. The attenuation of the pump is much larger than that in the previous case owing to the dissipation of the harmonics. Fig. 3(c) shows the signal transmission through a distance of $60\lambda_0$. Just as predicted, no parametric gain is realized.

2) Harmonic-Blocked Nonlinear Transmission Line: In this case and in the following experiment, we chose uniform impedance loads to be $Z_1 = Z_2 = 0.6$, with the denotations being defined in Fig. 1. A photonic band gap is formed at the third harmonic frequency of the pump in this case. When the transmission line is pumped at a wavelength of λ_0, the third harmonic turns out to be situated inside the band gap; no harmonics, therefore, can be progressively built up. Although this impedance loading violates the uniformity of the transmission line, the loaded transmission line can be approximately regarded as a homogeneous medium, since the perturbing distance is sufficiently smaller than the wavelength. We therefore have reasons to expect that the analytical results [11] are applicable in this case and can be verified by this numerical simulation.

First, we inspect the spatial traveling waveform for direct images of how the parametric amplification arises. The overall waveform propagating from left to right for a distance of $60\lambda_0$ is plotted in Fig. 4(a), in which it consists of the pump, the signal $f_s = 0.95$, and the image $f_i = 1.05$. The power of the signal is set to be -40 dB weaker than the pump at the input. After the pump is removed, the residual is shown in Fig. 4(b). This appears to be an amplitude modulation wave resulting from two-frequency beating. Then we separate the signal and the idler using the method given by (11) and (12) and plot their waveforms in Fig. 4(c) and (d), respectively. The most pronounced feature is the quasi-linear increase of the amplitude of the signal and the image. This is consistent with the quadratic manner of the power gain predicted by the analytical theory. Careful observation reveals that the signal does not start to gain power within the first several wavelengths until the image grows

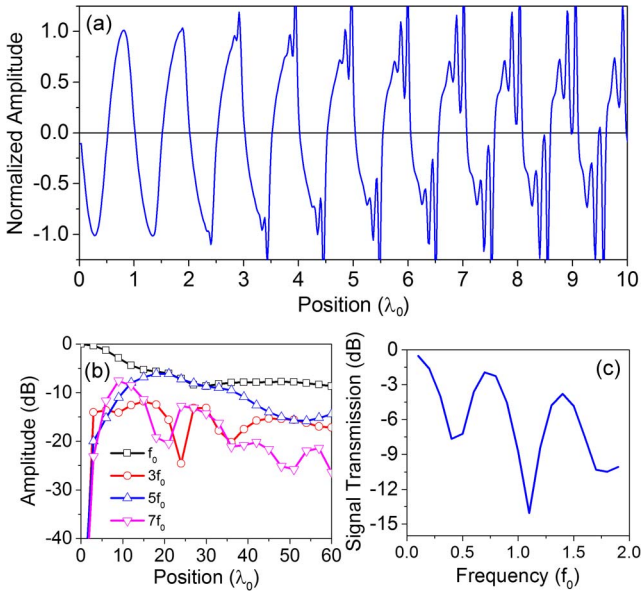

Fig. 3. Traveling-wave properties of an artificial transmission line with increasing parametric inductance $L = L_0(1 - \rho I^2)$. (a) Current waveform within the distance of the first $10\lambda_0$, driven by a sinusoidal oscillation at $z = 0$. (b) Amplitudes of the pump and its harmonics as a function of distance along the line. (c) Parametric gain as a function of signal frequency for a transmission distance of $60\lambda_0$ and nonlinear coefficient $\rho = 0.1$.

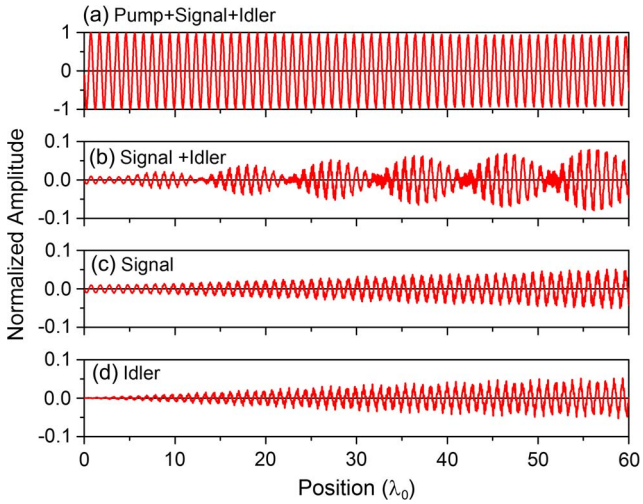

Fig. 4. Breakdown of waveforms of the traveling wave in a harmonic-blocked nonlinear superconducting transmission line with length of $60\lambda_0$ and nonlinear coefficient $\rho = 0.1$. (a) Overall waveform. (b) Residual waveform after removal of the pump. (c) Waveform of the signal. (d) Waveform of the idler.

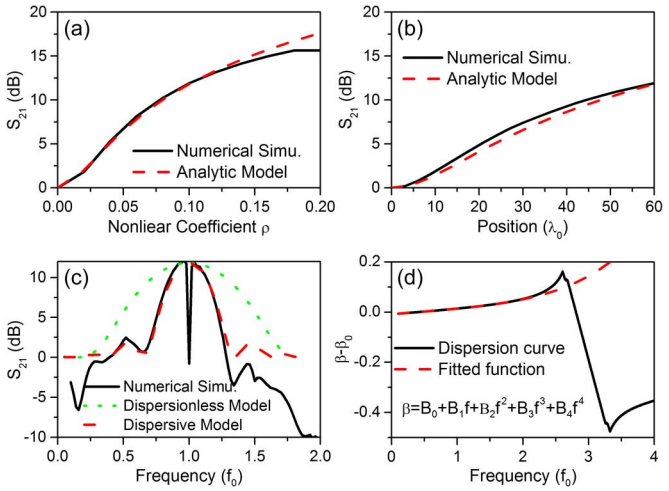

Fig. 5. Comparisons between the parametric gains obtained from the analytical model and the numerical simulation of a harmonic-blocked nonlinear superconducting transmission line. (a) Gain as a function of nonlinear coefficient with $L = 60\lambda_0$. (b) Gain as a function of distance with $\rho = 0.1$. (c) Gain bandwidth with $L = 60\lambda_0$ and $\rho = 0.1$. (d) Dispersion induced by the photonic band-gap structure and a fourth-order polynomial fitting model.

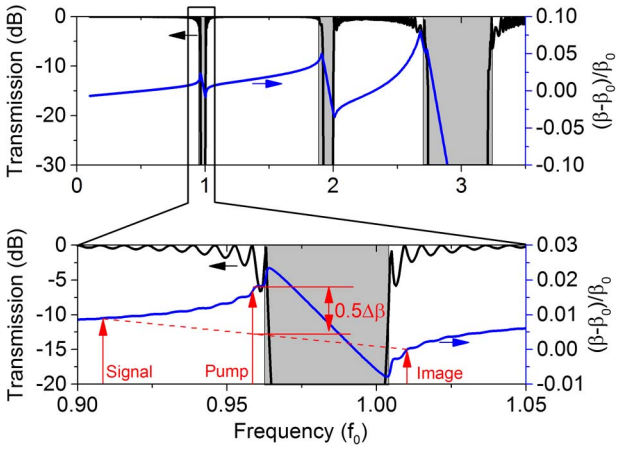

Fig. 6. Transmission and dispersion properties of a nonlinear superconducting transmission line with dispersion engineering. The lower part shows the details around the pump frequency. The realization of anomalous dispersion is illustrated.

to be a comparable amplitude to the signal. It is very notable that although the signal and the image become considerably strong, the overall waveform shown in Fig. 4(a) does not present any increase in amplitude. Empirically, it is because the composed waveform is nearly a frequency-modulated wave, since the phase of the wave shown in Fig. 4(b) is about 90° out of phase with the pump.

Then, we compare the analytical expectation with the numerical simulation of the parametric gain. On the one hand, the signal gain is numerically calculated as a function of the nonlinear coefficient ρ and the length of the transmission line $\mathscr{L}$ with the FDTD method. On the other hand, the dependence of the gain on ρ and $\mathscr{L}$ is derived from frequency-domain analysis; when $f_s \approx f_0$, it is

$$G_s = 1 + \left(\frac{\pi}{4}\rho\mathscr{L}\right)^2. \tag{13}$$

For the purpose of achieving quantitative agreement between them, we have to consider the fact that only the nonperturbed portions of the transmission line, where the linewidth is narrower, contribute to nonlinearity. In our design, this part is 80% of the overall length. The corrected length $\mathscr{L}' = 0.8\,\mathscr{L}$ is therefore adopted when calculating the signal gain using (13). The comparison is made in Fig. 5(a) and (b). Basically, the agreement can be met, except that there are some differences at relatively high nonlinearity, which is confirmed not owing to the depletion of the pump. The comparison of gain bandwidth is shown in Fig. 5(c). A significant difference in bandwidth occurs if the dispersion caused by the impedance perturbation is not taken into consideration. In fact, as shown in Fig. 5(d), the dispersion caused by the periodical impedance loading contributes significant linear dispersion, which narrows the bandwidth. This dispersion can be approximated by a polynomial fitting model, and we found that the polynomial of an order as high as 4 is needed to take account for the dispersion. With this dispersion taken into consideration, the gain can be calculated according to the Appendix. A good match of the analytical and simulated results is achieved when the gain is above 0 dB.

3) Nonlinear Transmission Line With Dispersion Engineering: Dispersion engineering [8], [10], [12] was introduced in addition to harmonic blockage for the purpose of generating anomalous dispersion $\Delta\beta = \beta_s + \beta_i - 2\beta_0 < 0$, which counteracts the nonlinear dispersion of the superconducting TWPA, i.e., $\rho/4$, so that the phase error $d\theta/dz = \Delta\beta + \rho/4$ can be reduced or even canceled out. If the phase-matching condition $d\theta/dz = 0$ is reached, an exponential gain can be obtained. At the band center, it is

$$G = \frac{1}{4}e^{\frac{\pi\rho\mathscr{L}}{2}}. \tag{14}$$

Dispersion engineering is performed in this study by setting $Z_1 = 0.6$ and $Z_2 = 0.8$. Making Z_2 differ from Z_1 introduces transmission notches around f_0 and the harmonics, as shown in Fig. 6. When the pump lies in the frequency range $0.90 < f_0 < 0.96$, the third harmonic tone of the pump falls inside the broad band gap at $3f_0$, and simultaneously, the linear dispersion $\Delta\beta$ is negative. Relatively large $\Delta\beta$ is only found in the frequencies close to the band gap. As shown in Fig. 6, the achievable value of $\Delta\beta$ is about 0.015. In comparison with the nonlinear dispersion $\rho/4 = 0.025$, the linear dispersion is not large enough to totally compensate the nonlinear one, and the gain, therefore, must be smaller than that given by (14). It is noted that the transmission periodically varies with the frequency in the vicinity of the band gap. The cause and consequent influence will be investigated further in the later part of this section.

The parametric gain is calculated by setting the pump at the frequency corresponding to the third maximum of transmission below the band gap. The result is plotted in Fig. 7 as a function of frequency, together with the gain profiles of the previously discussed two cases. Under the condition of using the same nonlinear coefficient $\rho = 0.1$, the gain will become significantly larger when applying dispersion engineering, but with a center gap, in which the transmission of either the signal or the image is blocked, as well as notable fluctuations at frequencies in the

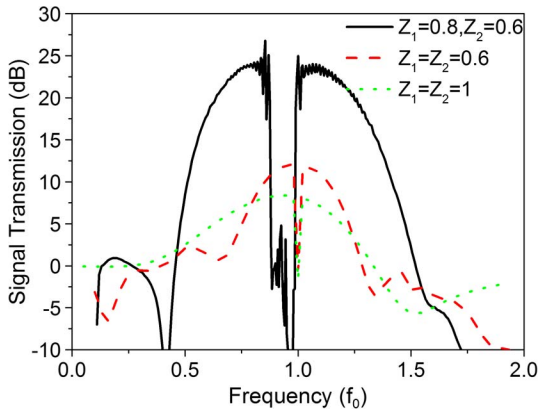

Fig. 7. Parametric gain profile of a nonlinear superconducting transmission line with application of dispersion engineering. The gain profiles of a uniform superconducting transmission line and a harmonic-blocked superconducting transmission line discussed previously are also plotted for comparison. For all the three cases, the nonlinear coefficients are the same, i.e., $\rho = 0.1$.

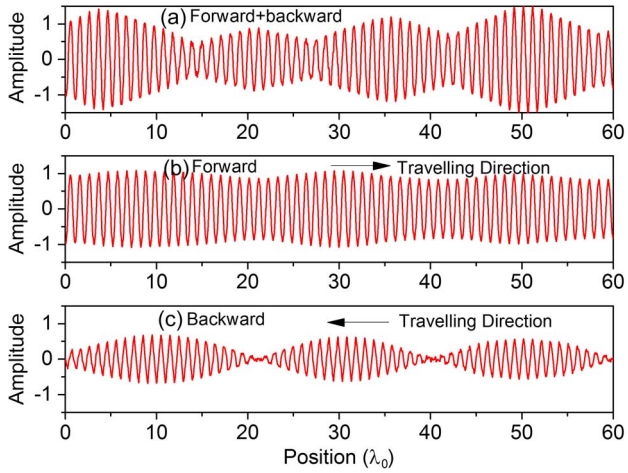

Fig. 8. Traveling pump waveforms in a nonlinear superconducting transmission line with application of dispersion engineering. The total length of the line is $60\lambda_0$, and the nonlinear coefficient is $\rho = 0.1$. (a) Overall waveform. (b) Forward traveling waveform. (c) Backward traveling waveform.

vicinity of the gap. The simulated gain profile is qualitatively consistent with the experimental results [8], [9] and the numerical results [13].

The application of dispersion engineering by impedance loading at every $\lambda_0/2$ violates the homogeneity of the transmission line more seriously than by periodical loading for harmonic blocking at the pump frequency. The reflection of waves taking place at the discontinuities of every $\lambda_0/2$ produces significant backward traveling waves, which cause the nonhomogeneity in the pump power distribution. This nonhomogeneity is illustrated in Fig. 8, where the pump frequency is set at the frequency corresponding to the third transition maximum outside the gap. The composed wave shown in Fig. 8(a) is an amplitude-modulated traveling wave. Unlike in the previous case shown in Fig. 4, where the amplitude of the pump traveling wave is almost uniform, the amplitude in this case is significantly modulated, in a range from the maximum amplitude of about 1.5 to the minimum amplitude of about 0.6. The nonuniformity in the current distribution causes the deviation of the nonlinear coefficient from varying with position and time, ranging from 0.225 to 0.036. To look further into it, we separate the forward and backward traveling waves using (11) and (12) and plot them in Fig. 8(b) and (c), respectively. The forward wave roughly keeps its amplitude along the line. However, the backward wave forms a well-defined coherently interfering pattern with three complete periods. Therefore, at the input port, the reflection is very small, and almost all the power is transferred to the output port. However, this full transmission does not indicate that the transmission medium behaves like a homogeneous line as in the previous case. It is therefore problematic to apply the analytical method to this case.

4) Standing Waves Caused by Impedance Mismatching: The measured gain profile in published works [8], [9] and the experimental results of this paper, to appear later, all present significant fluctuations in the gain profile. The gain fluctuations are mainly attributed to impedance mismatching at the input and output ports. As the fluctuations are troublesome in many practical applications, determination of the cause for the gain fluctuations is essential. For this purpose, the full S-parameter of the TWPA is necessary. In addition to the forward transmission coefficient S_{21}, which has been calculated for the parametric gain, we need to know the backward transmission coefficient S_{12} of this device. This is calculated using the FDTD method by introducing the signal from the output port and letting it travel to the input port, i.e., the opposite direction of the pump. The simulation results show that the signal travels backward through the line without noticeable attenuation despite the existence of the forward traveling pump. We, therefore, can write down the S matrix for a perfectly matched TWPA as

$$S = \begin{bmatrix} 0 & \sqrt{G_0(f)}e^{-j\beta_f \mathscr{L}} \\ e^{-j\beta_b \mathscr{L}} & 0 \end{bmatrix} \tag{15}$$

where $G_0(f)$ is the gain profile, and β_f and β_b are the signal propagation constants of the forward and backward waves, respectively. The fact that $|S_{12}|$ approximately equals to unity is a distinguished feature for this type of amplifier. In contrast to this direct feedback, semiconductor amplifiers usually have much larger isolation between output and input ports. This means that the internal feedback caused by the mismatching at the output and input ports can be very strong. Supposing the input and output of the reflection coefficients are Γ_i and Γ_o, respectively, and assuming that the intrinsic gain profile $G_0(f)$ is not significantly modified by the input/output mismatching, the gain profile can be calculated as

$$G(f) = \frac{G_0(f)\left(1-|\Gamma_i|^2\right)\left(1-|\Gamma_o|^2\right)}{\left|1+\sqrt{G_0(f)}\Gamma_i\Gamma_o e^{-j(\beta_f+\beta_b)\mathscr{L}}\right|^2}. \tag{16}$$

Because of the linear dependence of β_f and β_b on the frequency, the feedback phase in the denominator sweeps in the angular space periodically as the frequency changes. Consequently, positive and negative feedback alternatively appears. This results in a gain fluctuation of

$$\Delta G(f) = \left(\frac{1+\sqrt{G_0(f)}|\Gamma_i\Gamma_o|}{1-\sqrt{G_0(f)}|\Gamma_i\Gamma_o|}\right)^2. \tag{17}$$

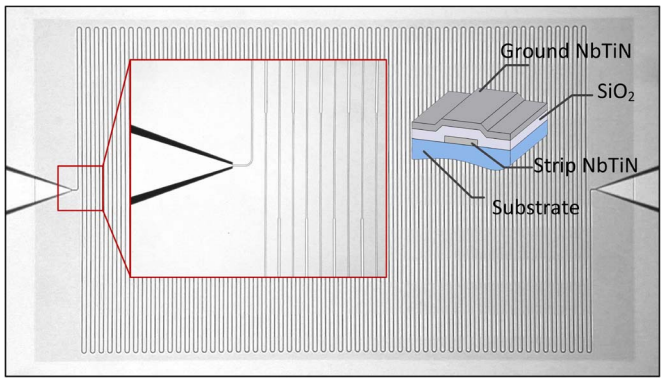

Fig. 9. Microscopic image of a microstrip TWPA. The frame of this photo is 4 mm × 2 mm. One of the insets shows the detail of the transition from the CPW line to the microstrip line. The other shows a schematic of the inversed microstrip line configuration.

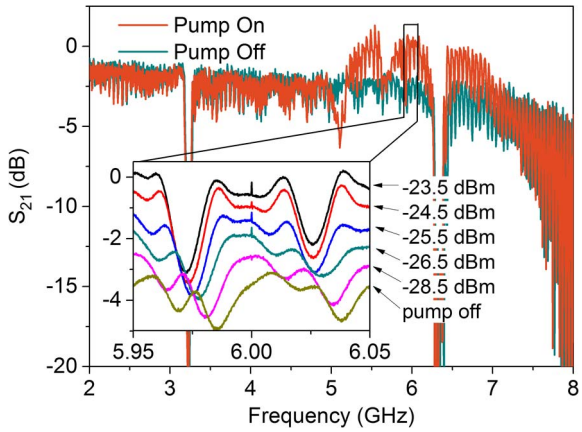

Fig. 10. Amplitude of the signal transmission coefficient of a microstrip TWPA as a function of frequency. The red and blue lines are $|S_{21}|$ with the pump power on and off, respectively. The inset shows the dependence of transmission on the pump power.

When

$$|\Gamma_i \Gamma_o| = \frac{1}{\sqrt{G_0(f)}} \tag{18}$$

the amplifier becomes unstable. For example, if the gain is 20 dB, and suppose that $\Gamma_i = \Gamma_o$, to keep the amplifier stable, the reflection coefficient should be less than 0.32, or SWR < 1.94. It is noted that even if the nonlinear transmission line is nominally matched at two ends, because of the aforementioned nonhomogeneity in a dispersion-engineered transmission line, a gain fluctuation still exists around the band center.

III. Experimental Methods

Microstrip line superconducting TWPAs have been fabricated to verify the feasibility of the fabrication process and demonstrate the parametric amplification. Fig. 9 shows the microscopic image of one sample. For simplicity in this feasibility study, only the periodic perturbations of impedance at an equal interval of $\lambda_0/6$ are performed to suppress the third harmonic generation, deferring dispersion engineering for future studies. The microstrip line consists of three layers of thin films, i.e., NbTiN/SiO_2/NbTiN, with nominal thickness of 30 nm/50 nm/30 nm, respectively. The strip width of the unperturbed sections is 1.5 μm, which results in a characteristic impedance of about 65 Ω. The effective characteristic impedance of the TWPA will be about 50 Ω if the perturbed sections are taken into consideration. The impedance is estimated according to Mattis–Bardeen theory, along with the fact that amorphous NbTiN is in the local extreme [19], [21], and assuming the film resistivity is 100 $\mu\Omega \cdot$ cm in the calculation. For the perturbed sections, the linewidth expands to 3 μm, and for each node, it extends to $\lambda_0/30$ in length. The overall length of the microstrip line is about 185 mm, which is nominally $60\lambda_0$ at 6 GHz. We employed an inversed microstrip layout shown in one of the insets in Fig. 9, in which the conducting strip is deposited prior to the ground plane. We consider that the conducting strip growing on the substrate will have better film quality in terms of Tc than on the deposited insulator. Another reason for that choice comes from the concern of possible weak links formed in the conducting strip because of the step coverage problem if we adopt the conventional microstrip configuration. The detailed fabrication method and parameters can be found elsewhere [22]. The inset in Fig. 9 shows the CPW–microstrip transition and an image of the perturbation of the linewidth. The chip size is 4 mm × 2 mm, which is much smaller than CPW TWPAs [8] owing to the slower wave speed in the microstrip line and the higher filling factor of this design.

Compared with monolayer CPW TWPAs, the fabrication of the trilayer microstrip type is more difficult. We suffered from limited insulation of the 50-nm-thick dielectric layer. The leakage of the insulator layer is believed to be caused by the static electric field breakdown during plasma etching or sputtering. Because of the large area of the device and the poor conductivity of NbTiN, static charges may easily accumulate to a hazardous voltage between the strip and the ground. Because of this problem, the yield is rather low (about 10%).

The TWPAs showing good insulation between the strip and the ground are screened and tested in a mechanic cryogenic Dewar at temperatures down to 3.8 K. The transmission coefficient is measured using a network analyzer. The pump, which was generated by a signal generator and adjusted by a step attenuator, is coupled to the device via a −20 dB broadband directional coupler. All cable losses are calibrated at cryogenic temperature before the devices are measured.

IV. Experiment Results and Discussion

The measured transmission coefficient of a microstrip TWPA is plotted in Fig. 10 as a function of frequency. The photonic band gap resulting from the impedance perturbation is centered at 8.8 GHz, which is much lower than the supposed 18 GHz. This is found to be due to the resistivity of the NbTiN film being as high as 250 $\mu\Omega \cdot$ cm, which is much larger than the designed 100 $\mu\Omega \cdot$ cm. This high resistivity results in a wavelength of 250 $\mu\Omega \cdot$ cm estimated according to Mattis-Bardeen theory, which is much larger than the designed 100 $\mu\Omega \cdot$ cm. The measured wavelength is 1505 μm at 6 GHz, consistent with the calculated result. The high resistivity also causes a high characteristic impedance of the microstrip line, which is estimated

to be 102 Ω, much larger than the designed 50 Ω. Therefore, impedance mismatching at the two ends of the microstrip line leads to a transmission fluctuation of about 2 dB. There are two unexpected narrow band gaps found around 3.2 and 6.4 GHz, respectively. Although the reason for these two gaps has not been identified, they are presumably caused by resonance modes of the parallel-plate chamber formed between the strip layer and the ground layer.

When a pump power of −23.5 dBm is applied to the transmission line at 6 GHz, a transmission enhancement as large as ∼4 dB can be observed around the pump frequency at 3.8 K physical temperature. This enhancement in transmission is evidently a parametric gain, although the absolute gain is only ∼1 dB in maximum because of the transmission loss. The magnitude of gain depends on the pump power, as shown in the inset in Fig. 10. It is verified that the gain depends on the pumping power in a quadratic manner, as predicted by (13). Despite the spurious band gap at 6.4 GHz as well as its image at 5.6 GHz, a continuous gain profile can be expected. It is noted that when the device is pumped at 6 GHz, its third harmonics lies in the second band gap resulting from the impedance perturbation.

An attenuation of the signal as large as 2 dB at 6 GHz was observed at 3.8 K. The transmission loss of the microstrip line at 3.8 K is measured to be $Q_0 = \beta/2\alpha = 2000$ at the frequency range of 7–8 GHz [22], where α is the attenuation coefficient. This Q value results in the transmission loss $\exp(-(\beta L/Q_0)) \approx 1.7$ dB at 6 GHz, which is comparable to the measured loss for the devices. The attenuation of pump reduces the nonlinearity significantly according to (3) and (14). Therefore, only the forepart of the transmission line, where the pump is not considerably attenuated, contributes the parametric gain, and the other part only contributes loss. We believe this is the cause for the low gain that was actually measured.

The nonlinearity coefficient was obtained by measuring the phase shift of S_{21} induced by the local oscillator power [23]. It results to be about $\rho = 0.03$, corresponding to the maximum pump power of about −23.5 dBm. Further increasing the pump power causes switching from the superconducting state to the normal state. Since the pump power is not uniform along the microstrip line, the measured nonlinearity coefficient is of averaged value. We, therefore, cannot estimate the gain quantitatively from (13), although the quadratic dependence of gain with pump power is still valid. The maximum pumping power is, in principle, determined by the critical current of the strip, but in practice, it is much lower because of the standing wave and defects in the strip where the superconductivity is weak. The existence of the standing wave reduces the maximum power of a perfectly matched transmission line by a factor of $(1-\Gamma_o)^2/(1+\Gamma_o)^2$, where Γ_o is the output refection coefficient. If dispersion engineering is employed, the maximum power can be further reduced because of the amplitude modulation of the traveling waves, as discussed previously.

V. Conclusion

We have investigated the parametric amplification in a nonlinear superconducting transmission line using a finite-difference method with second-order accuracy in both time and position. The progressive building of the signal and the image is visualized, providing a clear image of the principle of the amplifier. For a uniform nonlinear superconducting transmission line, parametric amplification happens even if shock waves occur. When shock waves are prevented by introducing a photonic band gap at the third harmonic of the pump, the wave propagation in the line becomes simpler. In this case, the numerical simulation results agree with the analytical results based on frequency-domain analysis. The parametric gain becomes considerably larger if the phase shift caused by nonlinearity is compensated completely or in part by applying the dispersion engineering technique. In this case, however, the transmission line can no longer be regarded as a homogeneous medium because of backward traveling waves arising due to the internal reflection caused by the inhomogeneity. The amplitude-modulated standing waves reduce the maximum applicable pump power and cause ripples in the gain profile at the band center even if both ends of the transmission line are matched. When the TWPA is not impedance matched at both ends, significant fluctuations in the gain profile occur because of the lack of isolation between the input and the output port. Impedance matching, therefore, is much more essential for the TWPA than for lumped-element amplifiers. Efforts have been made to fabricate NbTiN microstrip TWPAs, which are thought to be smaller in size and easier in broadband impedance matching compared with CPW TWPAs. Although the yield is very low, some devices survive, and parametric amplification was observed at a temperature of 3.8 K. The gain, no doubt, can be larger if the temperature goes down. Assessment in lower temperature and improvement in fabrication will be our future studies.

Appendix
Parametric Gain Bandwidth of the Dispersive Nonlinear Transmission Line

The expression for the signal gain is

$$G_s = |\cosh(gz)|^2 + \left|\frac{\kappa}{2g}\right|^2 |\sinh(gz)|^2 \tag{19}$$

where z is the distance, and

$$\kappa = \frac{\pi\rho}{2} + \Delta\beta \tag{20}$$

$$g^2 = \left(\frac{\pi\rho}{4}\right)^2 (1-\Delta f^2) - \frac{\kappa^2}{4} \tag{21}$$

$$\Delta\beta = \beta(f_0+\Delta f) + \beta(f_0-\Delta f) - 2\beta(f_0). \tag{22}$$

In the case of nondispersive media ($\Delta\beta = 0$), we have

$$G_s = 1 + \left(\frac{1}{\Delta f^2} - 1\right) \sin^2\left(\frac{\pi\rho}{4}\Delta f z\right). \tag{23}$$

If $\Delta f \approx 0$, we arrive at (13). In the case of dispersive media, (19) should be used instead of (23).

ACKNOWLEDGMENT

The authors would like to thank M. Sekine and T. Nitta of the National Astronomical Observatory of Japan (NAOJ) for their assistance in measurements, K. Matthias of NAOJ for helpful discussion on device fabrication, and J. Yang of the Purple Mountain Observatory for support in general.

REFERENCES

[1] H. Zimmer, "Parametric amplification of microwaves in superconducting Josephson tunnel junctions," *Appl. Phys. Lett.*, vol. 10, no. 7, pp. 193–195, 1967.

[2] P. T. Parrish and R. Y. Chiao, "Amplification of microwaves by superconducting microbridges in a four-wave parametric mode," *Appl. Phys. Lett.*, vol. 25, no. 10, pp. 627–629, 1974.

[3] M. J. Feldman, P. T. Parrish, and R. Y. Chiao, "Parametric amplification by unbiased Josephson junctions," *J. Appl. Phys.*, vol. 46, no. 9, pp. 4031–4042, 1975.

[4] M. A. Castellanos-Beltran, K. D. Irwin, G. C. Hilton, L. R. Vale, and K. W. Lehnert, "Amplification and squeezing of quantum noise with a tunable Josephson metamaterial," *Nature Phys.*, vol. 4, pp. 929–931, Oct. 2008.

[5] N. Bergeal *et al.*, "Phase-preserving amplification near the quantum limit with a Josephson ring modulator," *Nature*, vol. 465, pp. 64–68, May 2010.

[6] M. Hatridge, R. Vijay, D. H. Slichter, J. Clarke, and I. Siddiqi, "Dispersive magnetometry with a quantum limited SQUID parametric amplifier," *Phys. Rev. B, Condens. Matter*, vol. 83, no. 13, Apr. 2011, Art. no. 134501.

[7] E. A. Tholen *et al.*, "Nonlinearities and parametric amplification in superconducting coplanar waveguide resonators," *Appl. Phys. Lett.*, vol. 90, no. 25, 2007, Art. no. 253509.

[8] B. H. Eom, P. K. Day, H. G. LeDuc, and J. Zmuidzinas, "A wideband, low-noise superconducting amplifier with high dynamic range," *Nature Phys.*, vol. 8, pp. 623–627, Jul. 2012.

[9] C. Bockstiegel *et al.*, "Development of a broadband NbTiN traveling wave parametric amplifier for MKID readout," *J. Low Temp. Phys.*, vol. 176, no. 3, pp. 476–482, Aug. 2014.

[10] C. Macklin *et al.*, "A near-quantum-limited Josephson traveling-wave parametric amplifier," *Science*, vol. 350, no. 6258, pp. 307–310, Oct. 2015.

[11] J. Hansryd, P. A. Andrekson, M. Westlund, J. Li, and P.-O. Hedekvist, "Fiber-based optical parametric amplifiers and their applications," *IEEE J. Sel. Top. Quantum Electron.*, vol. 8, no. 3, pp. 506–520, May/Jun. 2002.

[12] K. O'Brien, C. Macklin, I. Siddiqi, and X. Zhang, "Resonant phase matching of Josephson junction traveling wave parametric amplifiers," *Phys. Rev. Lett.*, vol. 113, no. 15, Oct. 2014, Art. no. 157001.

[13] S. Chaudhuri, J. Gao, and K. Irwin, "Simulation and analysis of superconducting traveling-wave parametric amplifier," *IEEE Trans. Appl. Supercond.*, vol. 25, no. 3, Jun. 2015, Art. no. 150075.

[14] W. H. Press, S. A. Teukolsky, W. T. Vetterling, and B. P. Flannery, *Numerical Recipes in C*, 2nd ed. Cambridge, U.K.: Press Syndicate Univ. Cambridge, p. 842, Ch. 19, 1992.

[15] R. Landauer, "Parametric amplification along nonlinear transmission lines," *J. Appl. Phys.*, vol. 31, no. 3, pp. 479–484, 1960.

[16] S. A. Maas, *Microwave Mixers*. Norwood, MA, USA: Artech House, 1986, ch.7.

[17] R. Landauer, "Shock waves in nonlinear transmission lines and their effect on parametric amplification," *IBM J. Res. Develop.*, vol. 4, no. 4, pp. 391–401, 1960.

[18] V. Gaponov, L. A. Ostrovskii, and G. I. Freidman, "Electromagnetic shock waves," *Izvestiya VUZ. Radiofizika*, vol. 10, no. 9/10, pp. 1376–1413, 1967.

[19] R. L. Kautz, "Picosecond pulses on superconducting striplines," *J. Appl. Phys.*, vol. 49, no. 1, pp. 308–314, 1978.

[20] R. H. Pantell, "General power relationships for positive and negative nonlinear resistive elements," in *Proc. IRE*, vol. 46, no. 12, pp. 1910–1913, 1958.

[21] D. C. Mattis and J. Bardeen, "Theory of the anomalous skin effect in normal and superconducting metals," *Phys. Rev.*, vol. 111, no. 2, pp. 412–417, 1958.

[22] W. Shan, Y. Sekimoto, and T. Noguchi, "Microwave loss of DC sputtered NbTiN microstrip lines," *Japanese J. Appl. Phys.*, vol. 54, no. 9, Sep. 2015, Art. no. 090303.

[23] J. Gao *et al.*, "Properties of TiN for detector and amplifier applications," *J. Low Temp. Phys.*, vol. 176, no. 3, pp. 136–141, 2014.

Wenlei Shan (M'07) was born in Xi'an, China, in 1972. He received the B.Sc. and Ph.D. degrees in radio physics from Nanjing University, Nanjing, China, in 1995 and 2000, respectively.

He joined Purple Mountain Observatory (PMO), Chinese Academy of Sciences (CAS), Nanjing, as a Research Fellow in 2000. One year later, he moved to the Communication Research Laboratory of Japan, developing superconductor–insulator–superconductor (SIS) receiver systems. In 2003, he joined the Atacama Large Millimeter/submillimeter Array (ALMA) Group, National Astronomical Observatory of Japan (NAOJ), Tokyo, Japan, where he was responsible for the design and development of low-noise SIS mixers for ALMA band 8 and 10. In 2006, he moved to PMO as a Senior Researcher and developed a 9-pixel focal plane array SIS receiver at the 3-mm waveband for the Delinha 13.7-m telescope in China. In 2015, he moved back to NAOJ as an Associate Professor for developing next-generation focal plane array SIS receivers.

Yutaro Sekimoto received the Ph.D. degree in physics from The University of Tokyo, Tokyo, Japan, in 1994.

He is currently an Associate Professor with the National Astronomical Observatory of Japan (NAOJ), Tokyo. His current research interests include submillimeter-wave and cosmic microwave background instruments, superconductive detectors, and cosmology.

Takashi Noguchi was born in Saitama, Japan, in 1952. He received the B.S., M.S., and Ph.D. degrees from Tohoku University, Sendai, Japan, in 1976, 1978, and 1981, respectively, all in applied physics.

In 1981, he joined the Central Research Laboratory, Mitsubishi Electric Corporation, where he engaged in the research and development of superconducting devices for analog applications. He left Mitsubishi Electric Corporation in 1991 to join National Astronomical Observatory of Japan, Tokyo, Japan, where he worked on research and development of low-noise superconductor–insulator–superconductor (SIS) mixers for millimeter- and submillimeter-wave receivers and was in charge of development and production of SIS junctions for millimeter- and submillimeter-wave receivers of the Atacama Large Millimeter/submillimeter Array. His current research interest is the development of high-sensitivity superconductive detectors at submillimeter wavelengths.